ORIGINAL ARTICLE

Cancer Science WILEY

Driver gene alterations and activated signaling pathways toward malignant progression of gastrointestinal stromal tumors

Keiichi Ohshima[1,2] (iD) | Keiichi Fujiya[3] | Takeshi Nagashima[4,5] (iD) | Sumiko Ohnami[4] |
Keiichi Hatakeyama[1] (iD) | Kenichi Urakami[4,6] | Akane Naruoka[2] (iD) | Yuko Watanabe[1] |
Sachi Moromizato[1] | Yuji Shimoda[4,5] | Shumpei Ohnami[4] | Masakuni Serizawa[2] |
Yasuto Akiyama[7] | Masatoshi Kusuhara[2,6] | Tohru Mochizuki[1] | Takashi Sugino[8] |
Akio Shiomi[9] | Yasuhiro Tsubosa[10] | Katsuhiko Uesaka[11] | Masanori Terashima[3] |
Ken Yamaguchi[12]

[1]Medical Genetics Division, Shizuoka Cancer Center Research Institute, Shizuoka, Japan

[2]Drug Discovery and Development Division, Shizuoka Cancer Center Research Institute, Shizuoka, Japan

[3]Division of Gastric Surgery, Shizuoka Cancer Center Hospital, Shizuoka, Japan

[4]Cancer Diagnostics Research Division, Shizuoka Cancer Center Research Institute, Shizuoka, Japan

[5]SRL, Inc., Tokyo, Japan

[6]Region Resources Division, Shizuoka Cancer Center Research Institute, Shizuoka, Japan

[7]Immunotherapy Division, Shizuoka Cancer Center Research Institute, Shizuoka, Japan

[8]Division of Pathology, Shizuoka Cancer Center Hospital, Shizuoka, Japan

[9]Division of Colon and Rectal Surgery, Shizuoka Cancer Center Hospital, Shizuoka, Japan

[10]Division of Esophageal Surgery, Shizuoka Cancer Center Hospital, Shizuoka, Japan

[11]Division of Hepato-Biliary-Pancreatic Surgery, Shizuoka Cancer Center Hospital, Shizuoka, Japan

[12]Shizuoka Cancer Center Hospital and Research Institute, Shizuoka, Japan

Abstract

Mutually exclusive *KIT* and *PDGFRA* mutations are considered to be the earliest events in gastrointestinal stromal tumors (GIST), but insufficient for their malignant progression. Herein, we aimed to identify driver genes and signaling pathways relevant to GIST progression. We investigated genetic profiles of 707 driver genes, including mutations, gene fusions, copy number gain or loss, and gene expression for 65 clinical specimens of surgically dissected GIST, consisting of six metastatic tumors and 59 primary tumors from stomach, small intestine, rectum, and esophagus. Genetic alterations included oncogenic mutations and amplification-dependent expression enhancement for oncogenes (OG), and loss of heterozygosity (LOH) and expression reduction for tumor suppressor genes (TSG). We assigned activated OG and inactivated TSG to 27 signaling pathways, the activation of which was compared between malignant GIST (metastasis and high-risk GIST) and less malignant GIST (low- and very low-risk GIST). Integrative molecular profiling indicated that a greater incidence of genetic alterations of driver genes was detected in malignant GIST (96%, 22 of 23) than in less malignant GIST (73%, 24 of 33). Malignant GIST samples groups showed mutations, LOH, and aberrant expression dominantly in driver genes associated with signaling pathways of PI3K (*PIK3CA*, *AKT1*, and *PTEN*) and the cell cycle (*RB1*, *CDK4*, and *CDKN1B*). Additionally, we identified potential PI3K-related genes, the expression of which was upregulated (*SNAI1* and *TPX2*) or downregulated (*BANK1*) in malignant GIST. Based on our observations, we propose that inhibition of PI3K pathway signals

Correspondence
Keiichi Ohshima, Medical Genetics Division, Shizuoka Cancer Center Research Institute, Shizuoka, Japan.
Email: k.ohshima@scchr.jp

might potentially be an effective therapeutic strategy against malignant progression of GIST.

1 | INTRODUCTION

Gastrointestinal stromal tumors account for less than 1% of all gastrointestinal (GI) tumors and for approximately 5% of all sarcomas.[1] However, they are the most common (80%) mesenchymal tumors of the GI tract. Worldwide annual incidences are largely consistent, ranging between 11 and 19.6 per million population.[2] GIST originate from ICC or ICC-like stem cell precursors.[2] Age of onset ranges between teenage years to the 90s, with a peak onset age of 60 years.[3] The most common organ affected is the stomach (50%-60%) followed by small intestine (30%-35%), rectum (5%), and esophagus (<1%).[3] GIST often recur locally within the abdomen and/or are metastasized to the liver.[2] Prognosis for GIST has been assessed by risk stratification schemes, including the modified NIH classification.[4] This criterion, which considers tumor size, mitotic count, tumor location, and tumor rupture, is useful in identifying patients who might benefit from adjuvant therapy.[5]

Most GIST contain gain-of-function mutations in one of the two receptor tyrosine kinase genes, *KIT* (75%-80%) and *PDGFRA* (5%-10%), resulting in conformational changes of the respective proteins to constitutively activate downstream signaling pathways, including RAS/RAF/MAPK and PI3K/AKT/mTOR.[2] The remaining 10%-15% of GIST without *KIT* or *PDGFRA* mutations show different clinical and pathological features from the mutation-carrying GIST, and these so-called wild-type GIST include neurofibromatosis-type 1NF1, Carney triad, and Carney-Stratakis syndrome.[3] Discovery of TKI, including imatinib[6] and sunitinib,[7] targeting these oncogenic mutants, made a significant clinical impact on the drug treatment for GIST patients. Different types of mutations, including point mutations, deletions, and insertions can be found in the different exons of *KIT* and *PDGFRA*, and these mutations show type- and location-specific relationships with risk stratification, clinical manifestations, and drug response. For example, GIST patients carrying *KIT* exon 11 deletion mutations show poor prognosis,[8,9] but are sensitive to imatinib.[10] In *KIT*, oncogenic mutations found in exons other than exons 9 and 11 show primary resistance to imatinib, and some mutations in these regions arose from first-line treatment as secondary resistant mutations.[2,11] Thus, second- or third-line drug treatment is carried out for patients showing resistance to TKI.

Anderson et al and others have suggested that *KIT/PDGFRA* mutations are very common events in the early stage of GIST development, and are not sufficient for GIST progression, and that other genetic changes are required for clinical manifestation.[12-14] Several chromosomal changes, including deletions in chromosome arms 1p, 13q, 14q, 15q, and 22q,[14-17] and gains in chromosomes 4 and 5,[16,17]

have been associated with malignant progression of GIST. However, there are no consensus genetic alterations with mutations, amplification, or deletion for GIST development.[13] Thus, we aimed to identify driver gene alterations and the subsequent signaling pathways that drive the progression of GIST in order to develop effective therapies, particularly for TKI-resistant patients.

2 | MATERIALS AND METHODS

2.1 | Clinical samples

Tumor tissue samples dissected from surgical specimens, along with whole blood samples were obtained from Shizuoka Cancer Center under protocols approved by the institutional review board at Shizuoka Cancer Center (authorization number: 25-33).[18] Written informed consent was obtained from all patients enrolled in the study. All experiments using clinical samples were carried out in accordance with the approved guidelines.

2.2 | Sequencing analysis

Isolation and characterization of genomic DNA for WES and CCP has been described previously.[19,20] Exome library for WES was constructed using an Ion AmpliSeq Exome RDY Kit (Thermo Fisher Scientific). Briefly, 100 ng DNA was used in the target amplification under the following conditions: 99°C for 2 minutes, followed by 10 cycles at 99°C for 15 seconds and 60°C for 16 minutes, and a final hold at 10°C. Amplicons were ligated with Ion Torrent Proton adapters (Thermo Fisher Scientific) at 22°C for 30 minutes followed by 72°C for 10 minutes, and the library was purified with Agencourt AMPure XP beads (Beckman Coulter). This exome library supplied 293 903 amplicons that cover 57.7 Mb of the human genome, comprising 34.8 Mb exons of 18 835 genes registered in RefSeq. The constructed library was quantified using quantitative PCR, and DNA was sequenced using a semiconductor DNA sequencer (Ion Proton Sequencer; Thermo Fisher Scientific).

For CCP, the targeted DNA library comprising 1.6 Mb exon regions and splice sites of 409 genes was constructed using an Ion AmpliSeq Comprehensive Cancer Panel Kit (Thermo Fisher Scientific) with the Ion Library Equalizer Kit (Thermo Fisher Scientific). Briefly, 40 ng DNA was used for multiplex PCR amplification with four separate primer pools. The amplicons were treated with FuPa reagent (Thermo Fisher Scientific) and ligated to a uniquely barcoded adapter. After purification using Agencourt AMPure XP beads, the constructed library from each primer pool

was quantified using the Ion Library Quantification Kit (Thermo Fisher Scientific) and pooled together. Template preparation was carried out using the Ion Chef System (Thermo Fisher Scientific) and Ion PI Hi-Q Chef Kit (Thermo Fisher Scientific). DNA was sequenced using a semiconductor DNA sequencer (Ion Proton Sequencer).

Binary raw data derived from the semiconductor DNA sequencer were converted using Torrent Suite software (Thermo Fisher Scientific) into sequence reads that were mapped to the reference genome (UCSC hg19). At this step, sequence data derived from tumor and blood samples were saved as BAM files. Then, somatic mutation calling was applied separately for the WES and CCP datasets. For WES, two BAM files were uploaded to the Ion Reporter system and analyzed concurrently with AmpliSeq exome tumor-normal pair workflow (ver. 4.4; Thermo Fisher Scientific) with a Custom Hotspot file that specifies somatic and pathogenic mutations registered in COSMIC and ClinVar, respectively. The list of identified mutations was processed by in-house scripts to remove false-positive calls, including sequencer-derived errors. Mutations fulfilling at least one of the following criteria were discarded as false-positive: (i) quality score <60; (ii) depth of coverage <20; (iii) variant read observed in one strand only; (iv) clipped sequence length <100 (avg_clipped_length <100); (v) variant located on either sequence end (avg_pos_as_fraction <0.05); and (vi) mutation matches one on an in-house false-positive list. Parameters specified in criteria (iv) and (v) were calculated by bam-readcount with option "−q 1" (ver. 0.8.0) (https://github.com/genome/bam-readcount). For CCP, tumor CCP sequence reads were compared with blood WES reads to identify somatic mutations. First, variant calling for tumor samples was carried out using TVC (ver. 4.4; Thermo Fisher Scientific), and then blood data were analyzed by TVC with custom hotspot, which specifies all detected mutations in a tumor sample to determine whether these mutations were observed in the blood sample. Because a different variant caller and higher depth were used compared to those used for WES, the following criteria were used to identify unreliable mutations: (i) quality score <50; (ii) depth of coverage <20; or (iii) mutation matches one on an in-house false-positive list.

Effects of mutations were predicted using SnpEff.[21] Nonsynonymous mutations, including substitutions, insertions or deletions at coding regions and splice-sites were visually confirmed on the IGV,[22] and subsequently validated by Sanger sequencing. PCR and Sanger sequencing were carried out as described previously,[23] and primer sequences are shown in Table S1. Based on the number of WES reads, CNA was calculated according to the saasCNV method.[24] We defined gain and loss in the case of copy number as ≥2.5 and <1.5, respectively. WES data were applied to estimate tumor purity using an in silico method.[25] Data of SNV and INDEL from WES and CCP are listed in Data S1. CNA data from WES are listed in Data S2. For fusion gene analysis, total RNA was used as a template to prepare cDNA, and subjected to the Ion Proton System for detecting fusion transcripts from a panel of 491 fusion genes, as previously reported.[26]

2.3 | Gene expression analysis

Total RNA was isolated and subjected to microarray analysis as described previously[18] using SurePrint G3 Human Gene Expression 8 × 60K v2 Microarray (Agilent Technologies). RNA samples with RNA integrity number ≥5.9 were used for microarray analysis. Microarray analysis was carried out in accordance with the MIAME guidelines.[27] Data analysis was carried out using GeneSpring GX (Agilent Technologies), Subio platform (Subio), and Microsoft Excel. Probes to be analyzed were selected according to the reference genome sequence, hg19, obtained from the UCSC Genome Browser.[28] Raw signal intensity values were log-transformed and normalized to the 75th percentile. Microarray data for mRNA expression are available through the NCBI database under accession GSE136755.

2.4 | Statistical analysis

We used Fisher's exact test for comparison of two datasets. Welch's t test was carried out in the assumed normal distribution. P-values <0.05 were considered statistically significant. We used the Z-score, which indicates the number of standard deviations away from the mean of expression, to predict significant changes in gene expression.

3 | RESULTS

3.1 | Patient and tumor sample characteristics

A total of 65 surgically resected GIST tumor samples were obtained from 64 patients, which included six metastatic and 59 primary tumors (Table S2). One patient provided primary and matched metastatic tumor samples resected at a different time period. According to the risk criteria,[4] primary GIST tumor samples were divided into four groups with high (17 cases), intermediate (9 cases), low (22 cases) and very low (11 cases) risk of progression. Nine patients were treated with imatinib or sunitinib before surgery. With a combination of WES, targeted sequencing of 409 cancer-associated genes using the Ion AmpliSeq CCP, and Sanger sequencing (Tables S2 and S3), we identified oncogenic KIT and PDGFRA mutations in 57 (88%) and six (9%) of the 65 GIST samples, respectively. Among the KIT driver mutations, short deletions in exon 11 were observed more frequently ($P = 8.5 \times 10^{-3}$) in the metastatic/high-risk groups (15 of 23 tumors) than in the other risk groups (15 of 42 tumors), as reported previously.[8,9] In addition to the drivers, secondary KIT mutations,[2,11] including V654A in exon 13, T670I in exon 14, and N822Y in exon 17, were identified in three samples. CNA data by WES showed copy number gain of KIT in eight samples, of which a sample was from KIT/PDGFRA wild type (Figure S1). Three samples showed copy neutral loss of heterozygosity (cnLOH) in KIT. GEP showed that KIT mRNA expression levels were lower in samples harboring PDGFRA mutations than in those with KIT mutations ($P = 1.8 \times 10^{-2}$), whereas PDGFRA mRNA levels were lower in samples harboring KIT mutations than in samples with PDGFRA mutations ($P = 4.0 \times 10^{-4}$). These

observations were consistent with a previous report.[17] No correlation ($P = 2.8 \times 10^{-1}$) was observed in *KIT* expression levels between samples with (copy number ≥2.5) or without (copy number = 2) *KIT* copy number gain. Even excluding samples harboring *PDGFRA* mutations, this conclusion was unchanged ($P = 6.0 \times 10^{-1}$).

3.2 | Summary of WES and CCP

Mean depths of coverage for blood and tumor tissue sequences in WES were 131 (range, 94-164) and 126 (range, 93-126), respectively. In CCP, mean depth of tumor tissue sequences was 1183 (range, 851-1438). Total numbers of nonsynonymous mutations in WES and CCP were 1084 (mean, 16.7) and 213 (mean, 3.3), respectively. Among the 1084 mutations from WES, 113 mutations were derived from 409 CCP genes, and 85 out of 113 mutations (75.2%) were also detected in CCP. In contrast, 39.9% of mutations detected in CCP (85 out of 213) matched mutations detected by WES. Size of TMB, defined as the total number of synonymous/nonsynonymous mutations per megabase obtained from WES, ranged from 0.06 to 1.75 with a median of 0.77 (Figure S1), indicating no TMB-high (TMB ≥20) samples in this set of GIST samples.[19]

In addition to the GIST-initiating mutations of *KIT* and *PDGFRA*, we used WES and CCP data to investigate other genetic alterations against GIST progression, including SNV and INDEL of the 707 driver genes (Table S4 and Data S1) that were selected referring to several publications[29-31] and databases (COSMIC,[32] https://cancer.sanger.ac.uk/cosmic; Oncomine Comprehensive Assay v3, OCAv3, https://www.thermofisher.com/jp/ja/home/clinical/preclinical-companion-diagnostic-development/oncomine-oncology/oncomine-cancer-research-panel-workflow.html). Of these, 320 and 301 genes were defined as OG and TSG, respectively, and the remaining 86 genes had both characteristics. Among the 1084 mutations detected by WES, 128 mutations were derived from the 707 driver genes, and their presence was further confirmed by IGV analysis. We carried out CCP to enhance detection rate of driver gene mutations, as CCP gives more depth of coverage. Among the 213 mutations detected by CCP, 158 mutations were derived from the driver genes, 76 mutations of which were also detected by WES. For the 82 mutations uniquely detected by CCP, our validation by IGV confirmed the presence of only four mutations, including *FANCD2* (no. 8), *KIT* (nos 12 and 14), and *KMT2A* (no. 64) (Data S1B). Among the rest of the mutations, 42 out of 78 mutations (53.8%) were recurrently found mainly in the regions containing homopolymers and repetitive sequences, and primer-ends, suggesting false positivity. Excluding *KIT* and *PDGFRA* mutations, 68 driver gene mutations, consisting of 21 mutations defined as OG, 39 mutations defined as TSG, and eight mutations defined as OG/TSG, were used for further analysis.

3.3 | Oncogene mutations

In the case of the 406 OG, 29 mutations in 23 genes, consisting of 21 and eight mutations from 320 OG and 86 OG/TSG, respectively, were observed in 24 of the 65 samples (Figure 1). Among them, *PIK3CA* mutations, including G106R (observed in a metastatic sample, no. 1) and R88Q (observed in paired primary and metastatic samples, nos 6.1 and 6.2), were the only mutations that have been identified as activating mutations.[33,34] Of the remaining 26 mutations, *MUC4*, *HDAC1*, and *MUC16* mutations were found in multiple samples, but the mutation patterns in each gene were different. Additionally, we also carried out fusion gene analysis and identified the oncogenic *COL1A1-PDGFB* fusion transcript[35] in an intermediate-risk sample (no. 33) (Figure 1). Taken together, the observations in the two patients with either metastasis or high-risk GIST suggests that *PIK3CA* mutations are possible driver alterations for malignant progression of GIST.

3.4 | Tumor suppressor gene dysfunction by LOH

Oncogenes initiate carcinogenesis when mutations dominantly occur within a single copy of the gene, whereas TSG are required to follow Knudson's 'two-hit hypothesis' to recessively inactivate the gene.[36] In addition to the classical TSG inactivation, even partial TSG inactivation, as a result of haploinsufficiency, or dominant-negative TSG mutations could contribute to tumorigenesis.[36-38] TSG inactivation is also due to epigenetic mechanisms of gene silencing (eg, hypermethylation of CpG islands located in the promoter region).[39] Thus, we investigated TSG dysfunction considering the following categories: (i) LOH; (ii) deleterious mutations with expression reduction; (iii) haploinsufficiency/dominant-negative mutations; (iv) copy number loss accompanied by expression reduction; and (v) expression reduction without copy number loss.

First, we searched LOH-related TSG mutations among the 47 mutations, consisting of 39 and eight mutations from 301 TSG and 86 OG/TSG, respectively, using a combination of mutation and CNA data, and identified 15 mutations in 12 genes accompanied by copy number loss (copy number <1.5) (Figure 1, Data S2). Despite a lack of information on carcinogenesis, nonsense and frameshift mutations are predicted to be deleterious as a result of disruption of protein structure. According to the American College of Medical Genetics and Genomics (ACMG) standards and guidelines,[40] certain types of variant, including nonsense and frameshift, disrupt gene function by leading to a complete absence of the gene product by lack of transcription or NMD of an altered transcript. However, ACMG states that we must carefully interpret truncating variants to consider pathogenesis if the predicted stop codon occurs in the last exon or in the last 50 base pairs of the penultimate exon, in which NMD would not be predicted. Considering the locations, all the four nonsense mutations found in *RB1*, *MGA*, and *CBL* (Table 1) were predicted to be nonfunctional by NMD. However, it is unclear whether the missense mutations play tumor-suppressive roles. In addition, the effect of copy number loss on mRNA expression was assessed by GEP data. As summarized in Table 1, all of the seven deleterious mutations found in *RB1*, *PTEN*, *TSC1*, *MGA*, and *CBL* showed reduced expression levels (*Z*-score <0), which were designated as 'very likely' for TSG inactivation. One of the two *RB1* mutations was copy neutral LOH.
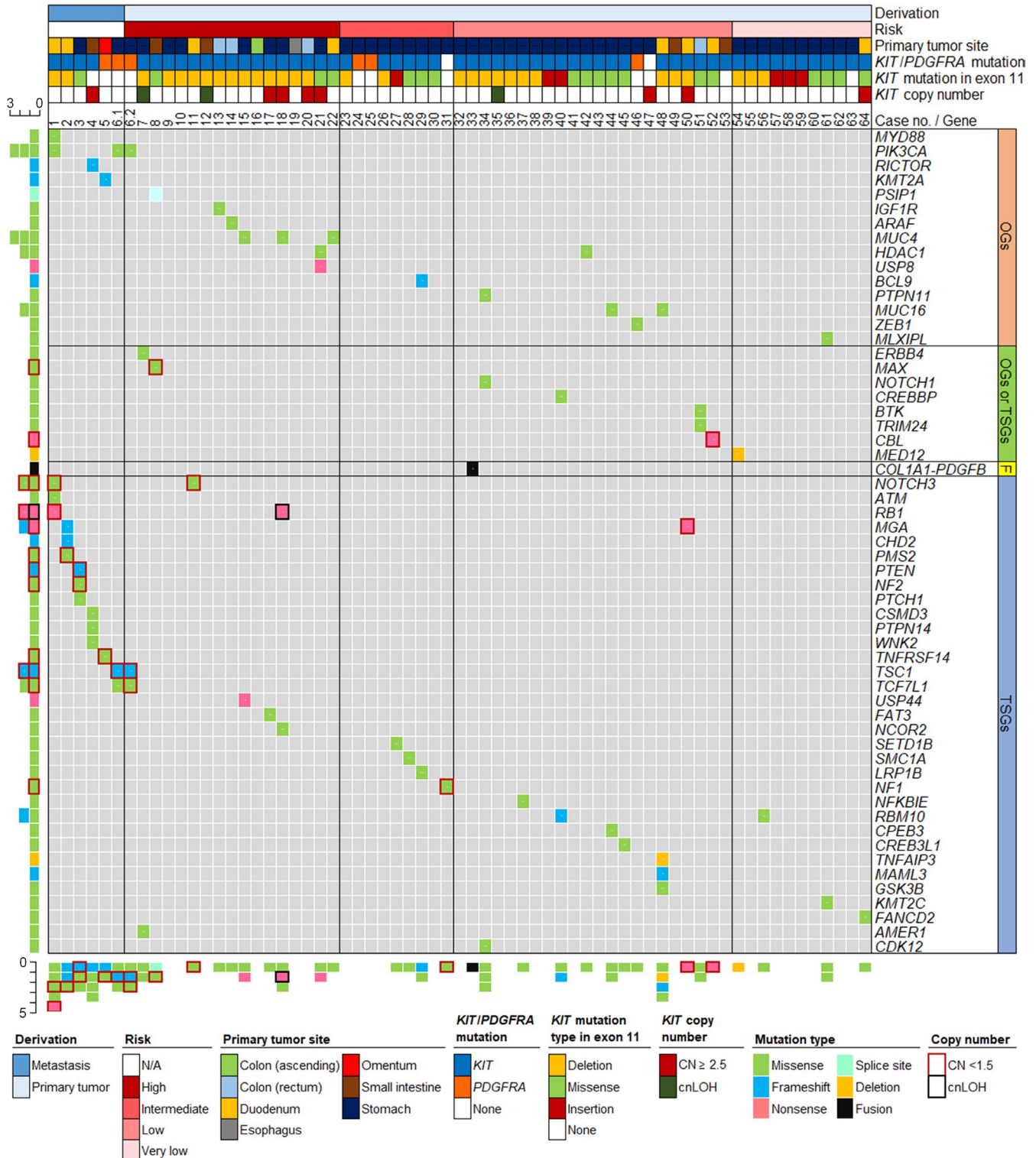
FIGURE 1 Driver gene mutations in 65 gastrointestinal stromal tumor (GIST) samples. Identified mutations of 707 driver genes, including oncogenes (OG) and tumor suppressor genes (TSG), and a fusion gene (F) are indicated. TSG mutations accompanied by loss of heterozygosity (LOH) are shown in red squares with copy number (CN) <1.5, and black squares with copy neutral LOH (cnLOH)

Eight missense mutations from seven genes, including *NOTCH3*, *PMS2*, *NF2*, *TNFRSF14*, *TCF7L1*, *MAX*, and *NF1*, were designated as 'possible'. Inactivation of *NF1* by LOH or other factors could have led to GIST in neurofibromatosis[41] in patient no. 31, in which no *KIT* and *PDGFRA* mutations were identified. LOH mutations

were observed in five metastatic, four high-risk, one intermediate, and two low-risk tumor samples. This indicated a higher rate of LOH presence in the metastatic/high-risk GIST samples than in the other samples ($P = 2.6 \times 10^{-3}$). In comparison with GIST derived from the stomach and other tissues, metastatic/high-risk

TABLE 1 Loss of heterozygosity (LOH)-driven tumor suppressor gene (TSG) inactivation

Case no.	Meta/Primary	Risk	Gene	Cytoband	Mutation Type	Allele	Site (coding DNA)	Site (protein)	Exon (exon position/no. of total exons)	Total length of protein (no. of amino acid residues)	Copy no.	Expression Signal	Z-score	Reduction (Z-score <0)[a]	Purity	Prediction of TSG inactivation[b]
1	Meta	NA	RB1	13q14.2	NS	hetero	c.649C > T	p.Q217*	7/27	928	1.44	1.12	-2.88	Yes	0.58	Very likely
1	Meta	NA	NOTCH3	19p13.12	MS	hetero	c.3658C > T	p.R1220W	22/33	2321	1.03	2.01	0.08	No	0.58	Possible
2	Meta	NA	PMS2	7p22.1	MS	hetero	c.958T > C	p.F320L	9/15	862	1.42	-0.52	-1.02	Yes	0.22	Possible
3	Meta	NA	PTEN	10q23.31	F	hetero	c.223_224delCA	p.H75fs	4/9	403	1.34	0.32	-2.58	Yes	0.51	Very likely
3	Meta	NA	NF2	22q12.2	MS	hetero	c.1414C > A	p.L472I	13/16	595	1.22	3.41	-0.74	Yes	0.51	Possible
5	Meta	NA	TNFRSF14	1p36.32	MS	hetero	c.17A > G	p.D6G	1/8	283	1.14	4.78	0.25	No	0.53	Possible
6.1	Meta	NA	TSC1	9q34.13	F	hetero	c.1360_1373delG TCACTCTAAGTGA	p.V454fs	14/23	1164	1.19	0.01	-3.67	Yes	0.29	Very likely
6.2	P	H	TSC1	9q34.13	F	hetero	c.1360_1373delGT CACTCTAAGTGA	p.V454fs	14/23	1164	0.86	0.47	-2.89	Yes	0.49	Very likely
6.2	P	H	TCF7L1	2p11.2	MS	hetero	c.887C > T	p.A296V	8/12	588	1.45	0.84	-0.57	Yes	0.49	Possible
8	P	H	MAX	14q23.3	MS	homo	c.108G > T	p.R36S	3/5	160	1.07	3.56	0.01	No	0.65	Possible
11	P	H	NOTCH3	19p13.12	MS	hetero	c.5707A > G	p.M1903V	31/33	2321	1.47	3.05	0.86	No	0.29	Possible
18	P	H	RB1	13q14.2	NS	homo	c.1324G > T	p.G442*	13/27	928	2 (cnLOH)	1.85	-1.64	Yes	0.56	Very likely
31	P	Int	NF1	17q11.2	MS	hetero	c.237A > T	p.L79F	3/58	2839	1.4	0.26	-2.14	Yes	0.19	Possible
50	P	L	MGA	15q15.1	NS	hetero	c.5654C > A	p.S1885*	17/24	3065	0.82	1.38	-1.17	Yes	0.34	Very likely
52	P	L	CBL	11q23.3	NS	hetero	c.891T > A	p.C297*	6/16	906	1.46	-0.67	-1.24	Yes	0.46	Very likely

Abbreviations: cnLOH, copy neutral LOH; F, frameshift; H, high; hetero, heterozygous; homo, homozygous; Int, intermediate; L, low; Meta, metastasis; MS, missense; NA, not available; NS, nonsense; P, primary.

[a]Expression level was deduced to be 'reduction' when Z-score was <0.

[b]TSG inactivation was predicted to be 'Very likely' with nonsense or frameshift mutations, and 'Possible' with missense mutation.

*Translation termination due to the presence of a stop codon.

GIST showed a higher proportion in tissues (65%, 13 of 20) other than the stomach (22%, 10 of 45; $P = 1.6 \times 10^{-3}$). Accordingly, the presence of LOH was higher in GIST from other tissues (35%, 7 of 20) than in GIST from the stomach (11%, 5 of 45; $P = 3.6 \times 10^{-2}$).

3.5 | Tumor suppressor gene dysfunction by other alterations

Among the five TSG harboring deleterious mutations without copy number loss (copy number ≥1.5), a frameshift mutation in *RBM10* showed reduced mRNA expression level (Table S5). This result indicates that mutation of *RBM10*, an RNA-binding protein and splicing regulator, has a tumor-suppressive role. Genes with the remainder of the four deleterious mutations, along with 27 genes harboring the missense and in-frame deletion mutations, can disrupt tumor-suppressive function of protein by haploinsufficiency or dominant-negative effect. However, according to the ACMG standards and guidelines[42] described previously, the nonsense *USP44* mutation was predicted to maintain its function as a result of its location on the penultimate exon. Thus, considering the types of mutations and locations, four deleterious mutations in *RBM10*, *CHD2*, *MGA*, and *MAML3* were designated as 'very likely' for TSG inactivation. However, these mutations may not directly contribute to tumor growth and progression of GIST, commonly referred to as passenger mutations.

Next, we integrated TSG inactivation by genes carrying copy number loss with expression reduction. This corresponds to TSG inactivation as a result of copy number loss in one of the alleles and expression reduction, due to epigenetic changes (eg, promoter methylation) in the other allele. TSG showing copy number loss (copy number <1.5) and expression reduction (Z-score ≤−2.5) were observed in 55 genes with a total of 66 alterations (Figure S2). Four of these cases were identified as LOH-related TSG (Table 1). In GIST, deletions in chromosome arms 1p, 13q, 14q, 15q, and 22q are frequently observed,[14-17] and were also observed in our samples (Figure S3). Particularly, our CNA data showed preferential copy number loss at 13q in the metastatic/high-risk GIST samples. Among the genes, expression reduction of *RB1* was observed in multiple cases, including in two metastatic and one high-risk tumors (Figure S2). This observation was consistent with the previous report that deletion at the *RB1* locus frequently occurred in recurrent or metastatic GIST.[43]

Last, we integrated TSG inactivation by genes showing expression reduction without copy number loss. This corresponds to TSG inactivation as a result of epigenetic modifications in both alleles. TSG showing expression reduction (Z-score ≤−2.5) without copy number loss (copy number ≥1.5) were observed in 112 genes with a total of 150 alterations (Figure S4). Seven genes, including *ASXL2*, *ARID1B*, *EXT1*, *CREB3L1*, *FANCF*, *NPRL3*, and *SMARCE1*, were downregulated in multiple samples of either metastatic or high-risk tumors. *TGFBR2*, *RUNX1TX*, *CDKN1B*, and *CDH1* showed expression reduction in multiple samples from either metastatic or high-risk tumors along with low-risk tumor samples.

3.6 | Oncogene amplification

Oncogenes are activated by mutations, amplification, and chromosomal rearrangements, causing either an alteration in oncogene structure or an increase in or deregulation of its expression.[44] In addition to mutation and fusion gene identification, amplification of OG were investigated. Our previous report showed that amplified genes are not always upregulated.[18] Thus, we integrated GEP data with CNA data to assess OG amplification. Among the 406 OG, 98 genes showed copy number gain (copy number ≥2.5) accompanied by expression enhancement (Z-score ≥1.5; Figure S5). Copy number gains of chromosomes 4 and 5 are frequently observed in GIST,[16,17] which were also shown in our samples (Figure S3). Additionally, our data showed gains of chromosome 20q in the metastatic/high-risk GIST samples, in which expression levels of *PLCG1*, *ZNF217*, and *GNAS* were enhanced in the metastatic or high-risk tumor samples. Other OG, which were identified in multiple tumor samples from independent metastatic/high-risk patients, included *SKP2*, *HOXA9*, *EZH2*, *CDK4*, *HMGA2*, and *FZD10*.

3.7 | Integration of activated OG and inactivated TSG

We summarized the activated OG and inactivated TSG in each tumor sample (Figure 2). Based on the types of alterations in OG and TSG, their effects on driver potential were classified into two types, including higher potential ('very likely') and lower potential ('possible'), as follows. The 'very likely' alterations were: (i) OG (*PIK3CA*) mutations known as activating mutations (Figure 1); (ii) OG amplified with increased expression (Figure S5); (iii) nonsense or frameshift TSG mutations with LOH (Table 1); (iv) frameshift TSG (*RBM10*) mutation with reduced expression (Table S5); (v) frameshift TSG mutations without reduced expression (Table S5); (vi) TSG with copy number loss and reduced expression (Figure S2); (vii) TSG with reduced expression (Figure S4); (viii) oncogenic fusion transcripts (Figure 1). The 'possible' alterations were: (i) OG mutations with unknown function (Figure 1); (ii) mutations found in genes defined as OG/TSG (Figure 1); (iii) missense TSG mutations with LOH (Table 1); (iv) missense TSG mutations (Figure 1). 'Very likely' driver gene alterations with showed higher incidence in the metastatic/high-risk GIST samples (96%, 22 of 23), including metastatic (100%, 6 of 6) and high-risk (94%, 16 of 17) tumors, than in the other risk GIST samples (73%, 24 of 33) of low- and very low-risk tumors ($P = 3.6 \times 10^{-2}$). In comparison with GIST derived from the stomach and other tissues, proportion of metastatic/high-risk GIST was higher in tissues (65%, 13 of 20) other than the stomach (28%, 10 of 36; $P = 1.1 \times 10^{-2}$). Accordingly, 'very likely' driver gene alterations were shown to be greater in GIST from other tissues (100%, 10 of 10) than from stomach GIST (72%, 26 of 36; $P = 9.5 \times 10^{-3}$).

The only metastatic/high-risk GIST sample in which no drivers were identified was a high-risk sample (no. 9). This sample remained without driver alterations even considering lower potential ('possible'). Besides the 707 driver genes, we investigated other genes with
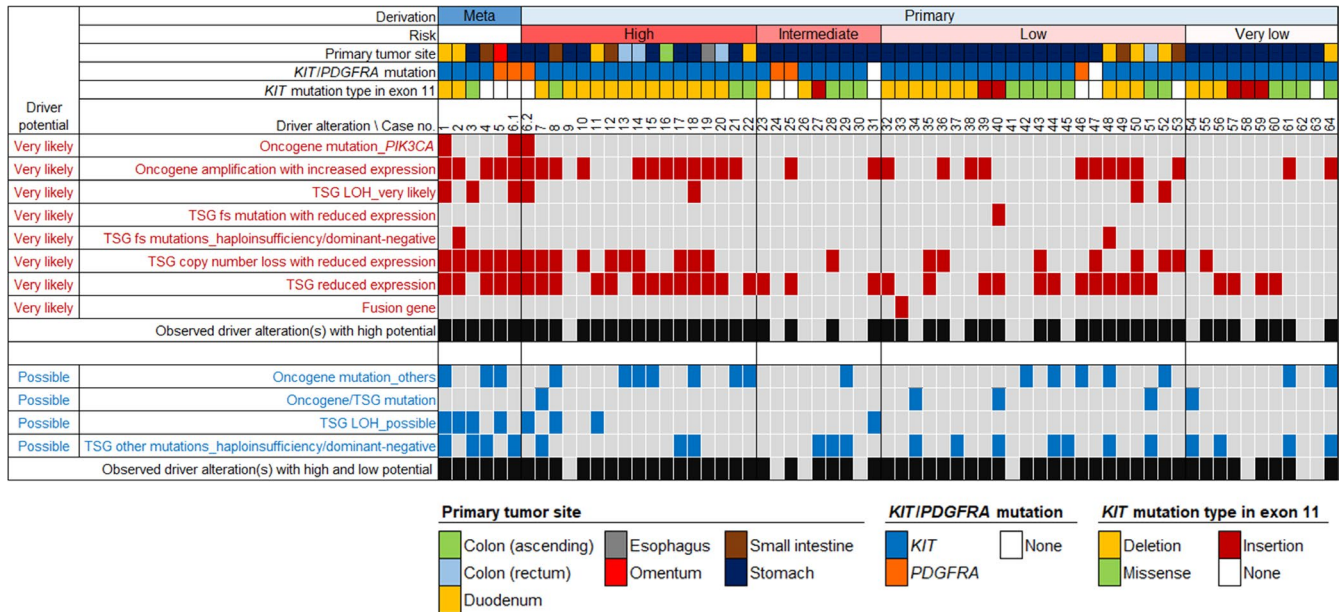
FIGURE 2 Summary of genetic alterations and expression modulations of driver genes. Alterations of driver potential were assigned and predicted by two different potential levels, including 'Very likely' and 'Possible' levels, which are shown in red and blue, respectively. LOH, loss of heterozygosity; TSG, tumor suppressor gene

driver potential in sample no. 9 by comparing GEP data between the metastatic/high-risk GIST and the other risk GIST (low- and very low-risk) samples (Figure 3A). To identify potential OG, 14 genes showing copy number gain (copy number ≥2.5) and expression enhancement (Z-score ≥1.0) in sample no. 9 were extracted from the genes significantly upregulated (fold change ≥2, $P < .05$) in the metastatic/high-risk GIST samples (Figure 3B). The 14 upregulated genes were located on chromosomes 4q or 20q, where copy number was gained in sample no. 9 (Figure S3). As a potential TSG, only *BANK1* was extracted as a gene showing expression reduction in sample no. 9 among the genes significantly downregulated (fold change ≤0.5, $P < .05$) in the metastatic/high-risk GIST samples (Figure 3B). For all 15 potential driver genes, no significant difference in expression level was observed between the metastatic and high-risk tumors ($P > .05$).

3.8 | Signaling pathway activation

Understanding of the genes along with pathways altered in tumor samples is essential to identify potential therapeutic options and vulnerabilities. According to the published information,[30,31] we determined a pathway related to each driver gene (Table S4). Then, we assigned driver genes with alterations as 'very likely' driver potential (Figure 2) to 27 pathways. Genetic alterations in the pathways of HIPPO, WNT, PI3K, NOTCH, cell cycle, and RAS-MAPK were observed in 10 or more samples (Figure 4A). By comparing the alteration frequency, PI3K and cell cycle pathways were significantly ($P = 2.1 \times 10^{-2}$) altered in the metastatic/high-risk GIST samples (metastatic and high-risk tumors) than in the other risk GIST samples (low- and very low-risk tumors (Figure 4B). Despite statistical nonsignificance, alteration in the chromatin SWI/SNF

complex pathway was found in five samples, all of which were derived from the metastatic/high-risk tumor samples. In all the samples, the presence of deletion mutations in *KIT* exon 11 was not significantly related to alterations in PI3K and cell cycle pathways ($P = 3.8 \times 10^{-1}$, $P = 7.4 \times 10^{-1}$, respectively). Also, in the metastatic/high-risk tumor samples, no correlations between them were found ($P = 4.0 \times 10^{-1}$, $P = 1.8 \times 10^{-1}$, respectively). The PI3K pathway has been reported to be activated as a result of imatinib secondary resistance.[42,45,46] In the present study, we observed PI3K pathway alteration even in tumor samples derived from patients not treated with neoadjuvant imatinib. In the metastatic/high-risk tumor samples, the alterations in PI3K and cell cycle pathways were not significantly related to neoadjuvant imatinib ($P = 4.1 \times 10^{-1}$, $P = 4.2 \times 10^{-1}$, respectively).

4 | DISCUSSION

KIT or *PDGFRA* mutations activate most GIST (~90%). However, their prognosis and development are independent of the types of mutation. Thus, these mutations are believed to be early events in GIST development, which involves additional genetic alterations for malignant progression.[12-14] Saponara et al reported that metastatic GIST showed frequent copy number loss at regions located on TSG, although no shared oncogenic mutations were observed except in *KIT*.[13] In the present study, despite the fact that there were no common mutations in driver genes of GIST with the maximum frequency of 5%, we showed that PI3K and cell cycle signaling pathways were involved in GIST malignant progression.

KIT and *PDGFRA* oncogenic mutations activate downstream signaling pathways, including RAS/MAPK, PI3K/AKT, and STAT3.[2]
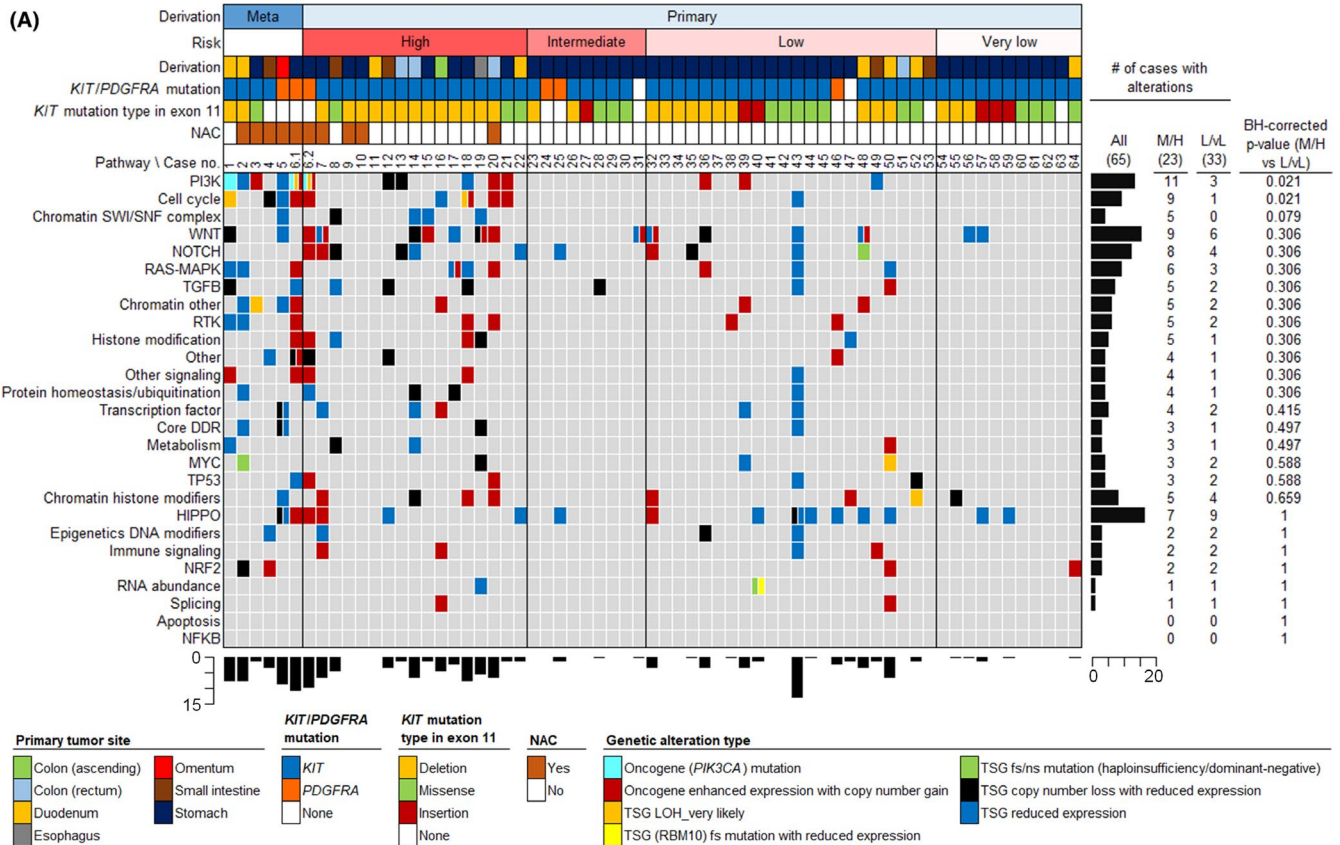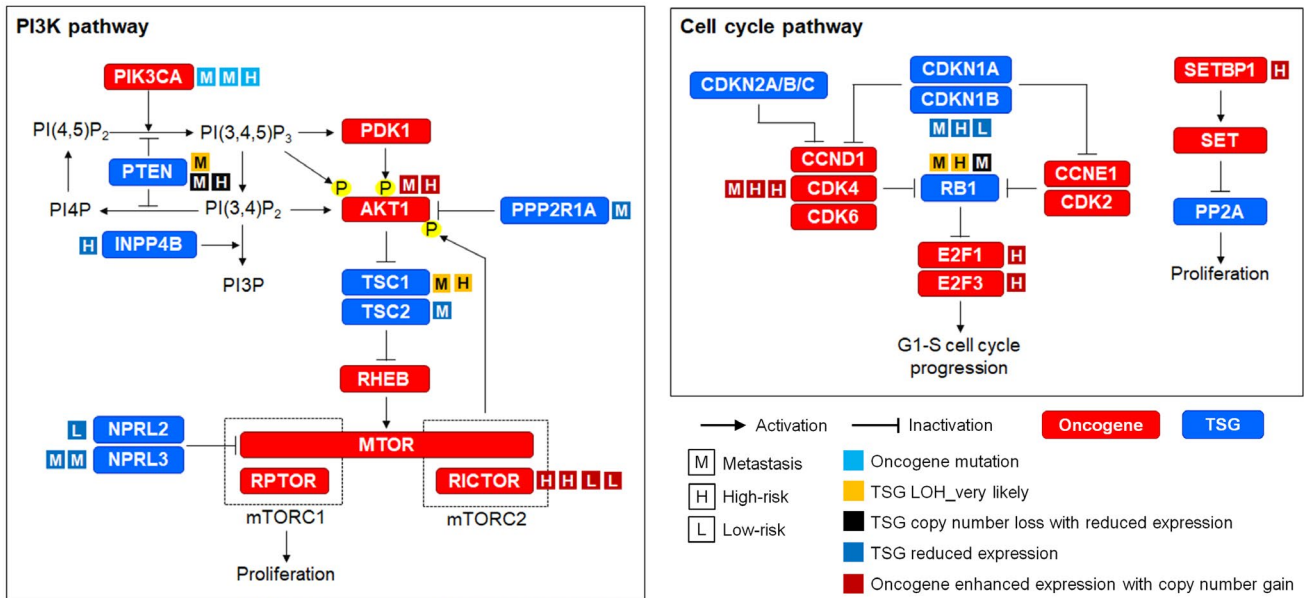
FIGURE 3 Identification of oncogenic or tumor-suppressive candidate genes. A, Volcano plot showing differentially expressed genes between two groups with different degrees of malignant progression, consisting of metastasis (M) and high-risk (H), and low (L) and very low (vL) risk. All circles represent 25 434 microarray probes corresponding to mRNA; closed and open circles for probes showing copy number (CN) ≥2.5 in sample no. 9 with expression levels of Z-score ≥1.0 and Z-score <1.0, respectively. Closed triangle indicates probe showing expression reduction with Z-score ≤−2.5 in sample no. 9. Gray circles indicate other probes. Log₂ fold change in the H/M versus L/vL is represented on the x-axis. The y-axis shows the log₁₀ of the Q value. A Q value of 0.05 and a fold change of 2 are indicated by horizontal and vertical dotted lines, respectively. B, Z-score expression levels of 15 genes in 65 GIST tumor samples. Probes corresponding to these genes were selected as copy number ≥2.5 and Z-score ≥1.0 in sample no. 9 (closed circles in Figure 3A) or as Z-score ≤−2.5 in sample no. 9 (closed triangle in Figure 3A) among the probes showing differential expression in the M/H group. C, Expression and copy number levels of 15 genes. In each panel, the open red circle represents sample no.9 and closed red circles represent other samples that belong to the M/H group. Gray squares and blue circles represent the intermediate-risk (Int) and L/vL groups, respectively.

Saponara et al reported frequent inactivation of tumor-suppressive *PTEN*, which is involved in the PI3K pathway, as a result of LOH or copy number loss with expression reduction in metastatic GIST.[13]

In addition to LOH of *PTEN*, we dominantly identified genetic alterations of PI3K pathway genes in malignant GIST samples with metastatic or high-risk group, including oncogenic activation by *PIK3CA*

FIGURE 4 Curated pathways. A, Genetic alterations and expression modulations found in the 27 pathways for each gastrointestinal stromal tumor (GIST) sample. On the right, frequency of pathway involvement was compared between two groups with different degrees of malignant progression, consisting of metastasis (M) and high-risk (H), and low (L) and very low (vL) risk. B, Pathway members and interactions in the PI3K and cell cycle pathways. LOH, loss of heterozygosity; TSG, tumor suppressor gene

mutations and copy number gain with expression enhancement in *AKT1* and *RICTOR*, and tumor-suppressive inactivation by LOH or expression reduction of *TSC1/2*, and *NPRL3* (Figure S6). The PI3K pathway has been reported to be activated as a result of imatinib

secondary resistance, including GIST.[42,45,46] In the present study, we observed PI3K pathway alteration even in tumor samples derived from patients who were not treated with neoadjuvant imatinib, suggesting that PI3K activation was irrelevant to imatinib treatment in
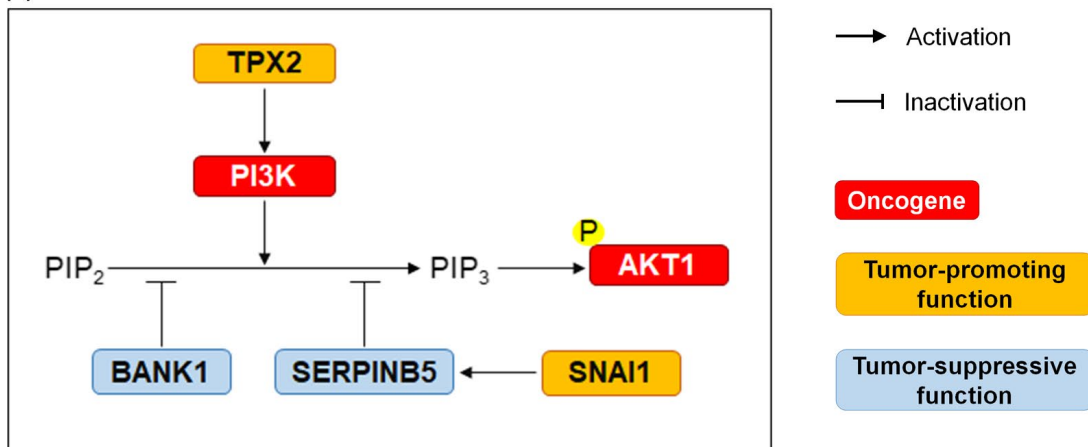
(A)
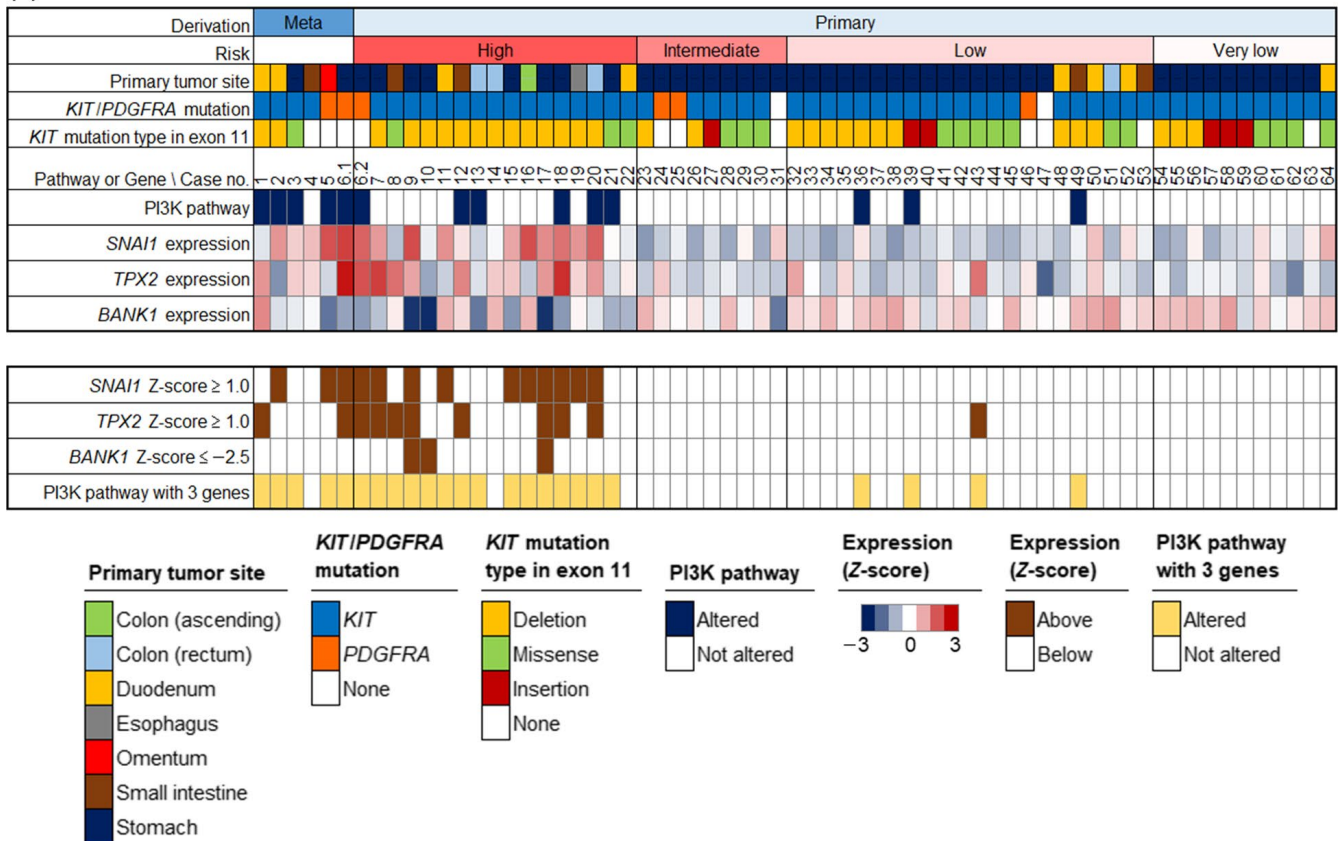
(B)

FIGURE 5 Genetic alterations and expression modulations of PI3K pathway-related genes. A, Expression levels of *SNAI1*, *TPX2*, and *BANK1*. Expression data were added to the data on the PI3K pathway shown in Figure 4A. B, Overview of the PI3K pathway with involvement of *SNAI1*, *TPX2*, and *BANK1*. Interactions between genes were deduced based on published articles.[50,51,53]

metastatic and high-risk GIST. Also, no correlation was observed between KIT exon 11 deletions and PI3K activation.

Our observations indicated that the cell cycle was another pathway showing genetic alterations significantly observed in metastatic and high-risk GIST. Reduced mRNA expression of tumor-suppressive *CDKN2A* gene leads to upregulation of *E2F1*, increasing cell proliferation to drive poor prognosis for GIST.[47] Saponara et al reported that copy number losses of *CDKN2A* and *CDKN2B* were the most frequent in metastatic GIST.[13] We also observed significant losses of *CDKN2A*

and *CDKN2B* in metastatic and high-risk GIST compared with the other risk GIST ($P = 6.4 \times 10^{-3}$). However, as a result of insufficient decreased mRNA levels, these genes were not identified as altered TSG. Inactivating mutations of other cell cycle pathway genes, including *RB1* and *TP53*, occur in high-risk GIST, showing activation of the cell cycle pathway.[48,49] We also observed inactivation of *RB1*, but not of *TP53*. *CDKN1B*, another TSG, was downregulated in two samples from each metastasis and high-risk GIST group. As *CDKN1B* is suppressed by *AKT*,[2] the cell cycle pathway can cooperate with the PI3K pathway.

We identified 15 potential driver genes from a GIST sample (no. 9) without alterations in the 707 known driver genes. Analysis of associated pathways showed that *SNAI1*, *TPX2*, and *BANK1* were involved in the PI3K pathway. *SNAI1*, a zinc-finger transcription factor, promoted cell migration through downregulation of *SERPINB5* (Maspin) and subsequent activation of PI3K/AKT-dependent Rac1 during prostate cancer progression.[50] *TPX2*, targeting protein for Xklp2, which is a microtubule-associated protein, suppressed proliferation through repressing the PI3K/AKT signaling pathway in breast cancer cells.[51] Downregulation of *BANK1* promoted CD40-dependent AKT activation in B cells.[52,53] Collectively, in sample no. 9, *SNAI1* and *TPX2* were activated by amplification-dependent expression enhancement, and *BANK1* was inactivated by expression reduction. Among other metastatic/high-risk GIST, 12 and nine samples were upregulated (Z-score ≥1.0) without copy number gain for *SNAI1* and *TPX2*, respectively (Figure 5A). Two more metastatic/high-risk GIST showed reduced expression (Z-score ≤−2.5) of *BANK1*. Based on activated AKT (Figure 5B), insertion of these results into the alteration data identified that 20 (87%) of the 23 metastatic/high-risk samples were involved in the PI3K pathway, suggesting that its activation drives malignant progression of GIST. In fact, the PI3K pathway has been implicated in metastasis for various types of tumors (review in ref[54]).

In summary, using multi-omics analysis, we identified driver gene alterations and subsequent signaling pathways. Our data indicate that the PI3K and cell cycle pathways play important roles in GIST malignant progression, which can be of significance for prognosis and treatment of GIST. Particularly, we propose that the development of PI3K inhibitors[55] is of potential benefit for patients with metastatic/high-risk GIST.

ACKNOWLEDGMENTS

DISCLOSURE

Authors declare no conflicts of interest for this article.

ORCID

Keiichi Ohshima (iD) https://orcid.org/0000-0002-2882-7566

Takeshi Nagashima (iD) https://orcid.org/0000-0002-7261-9908

Keiichi Hatakeyama (iD) https://orcid.org/0000-0001-6000-5899

Akane Naruoka (iD) https://orcid.org/0000-0002-6401-0318

REFERENCES

1. Zhao X, Yue C. Gastrointestinal stromal tumor. *J Gastrointest Oncol*. 2012;3:189-208.
2. Corless CL, Barnett CM, Heinrich MC. Gastrointestinal stromal tumours: origin and molecular oncology. *Nat Rev Cancer*. 2011;11:865-878.
3. Joensuu H, Hohenberger P, Corless CL. Gastrointestinal stromal tumour. *Lancet*. 2013;382:973-983.
4. Joensuu H. Risk stratification of patients diagnosed with gastrointestinal stromal tumor. *Hum Pathol*. 2008;39:1411-1419.
5. Rutkowski P, Bylina E, Wozniak A, et al. Validation of the Joensuu risk criteria for primary resectable gastrointestinal stromal tumour - the impact of tumour rupture on patient outcomes. *Eur J Surg Oncol*. 2011;37:890-896.
6. Demetri GD, von Mehren M, Blanke CD, et al. Efficacy and safety of imatinib mesylate in advanced gastrointestinal stromal tumors. *N Engl J Med*. 2002;347:472-480.
7. Demetri GD, van Oosterom AT, Garrett CR, et al. Efficacy and safety of sunitinib in patients with advanced gastrointestinal stromal tumour after failure of imatinib: a randomised controlled trial. *Lancet*. 2006;368:1329-1338.
8. Andersson J, Bümming P, Meis-Kindblom JM, et al. Gastrointestinal stromal tumors with KIT exon 11 deletions are associated with poor prognosis. *Gastroenterology*. 2006;130:1573-1581.
9. Hou YY, Grabellus F, Weber F, et al. Impact of KIT and PDGFRA gene mutations on prognosis of patients with gastrointestinal stromal tumors after complete primary tumour resection. *J Gastrointest Surg*. 2009;13:1583-1592.
10. Heinrich MC, Corless CL, Demetri GD, et al. Kinase mutations and imatinib response in patients with metastatic gastrointestinal stromal tumor. *J Clin Oncol*. 2003;21:4342-4349.
11. Nishida T, Kanda T, Nishitani A, et al. Secondary mutations in the kinase domain of the KIT gene are predominant in imatinib-resistant gastrointestinal stromal tumor. *Cancer Sci*. 2008;99:799-804.
12. Anderson W, O'Sullivan B, Hughes F, et al. Microscopic gastrointestinal stromal tumours: a clinical and molecular study of 13 cases. *Histopathology*. 2017;70:211-216.
13. Saponara M, Urbini M, Astolfi A, et al. Molecular characterization of metastatic exon 11 mutant gastrointestinal stromal tumors (GIST) beyond KIT/PDGFRα genotype evaluated by next generation sequencing (NGS). *Oncotarget*. 2015;6:42243-42257.
14. Schaefer I-M, Wang Y, Liang C-W, et al. MAX inactivation is an early event in GIST development that regulates p16 and cell proliferation. *Nat Commun*. 2017;8:14674.
15. El-Rifai W, Sarlomo-Rikala M, Andersson LC, et al. DNA sequence copy number changes in gastrointestinal stromal tumors: tumour progression and prognostic significance. *Cancer Res*. 2000;60:3899-3903.
16. Astolfi A, Nannini M, Pantaleo MA, et al. A molecular portrait of gastrointestinal stromal tumors: an integrative analysis of gene expression profiling and high-resolution genomic copy number. *Lab Invest*. 2010;90:1285-1294.
17. Schoppmann SF, Vinatzer U, Popitsch N, et al. Novel clinically relevant genes in gastrointestinal stromal tumors identified by exome sequencing. *Clin Cancer Res*. 2013;19:5329-5339.
18. Ohshima K, Hatakeyama K, Nagashima T, et al. Integrated analysis of gene expression and copy number identified potential cancer driver genes with amplification-dependent overexpression in 1,454 solid tumors. *Sci Rep*. 2017;7:641.
19. Hatakeyama K, Nagashima T, Urakami K, et al. Tumour mutational burden analysis of 2,000 Japanese cancer genomes using whole exome and targeted gene panel sequencing. *Biomed Res*. 2018;39:159-167.
20. Hatakeyama K, Ohshima K, Nagashima T, et al. Molecular profiling and sequential somatic mutation shift in hypermutator tumours harbouring POLE mutations. *Sci Rep*. 2018;8:8700.
21. Cingolani P, Platts A, Wang LL, et al. A program for annotating and predicting the effects of single nucleotide polymorphisms, SnpEff:

SNPs in the genome of Drosophila melanogaster strain w1118; iso-2; iso-3. *Fly*. 2012;6:80-92.

22. Robinson JT, Thorvaldsdóttir H, Winckler W, et al. Integrative genomics viewer. *Nat Biotechnol*. 2011;29:24-26.

23. Serizawa M, Kusuhara M, Ohnami S, et al. Novel tumor-specific mutations in receptor tyrosine kinase subdomain IX significantly reduce extracellular signal-regulated kinase activity. *Anticancer Res*. 2016;26:2733-2744.

24. Zhang Z, Hao K. SAAS-CNV: a joint segmentation approach on aggregated and allele specific signals for the identification of somatic copy number alterations with next-generation sequencing data. *PLoS Comput Biol*. 2015;11:e1004618.

25. Larson NB, Fridley BL. PurBayes: estimating tumor cellularity and subclonality in next-generation sequencing data. *Bioinformatics*. 2013;29:1888-1889.

26. Urakami K, Shimoda Y, Ohshima K, et al. Next generation sequencing approach for detecting 491 fusion genes from human cancer. *Biomed Res*. 2016;37:51-62.

27. Brazma A, Hingamp P, Quackenbush J, et al. Minimum information about a microarray experiment (MIAME)-toward standards for microarray data. *Nat Genet*. 2001;29:365-371.

28. Kent WJ, Sugnet CW, Furey TS, et al. The human genome browser at UCSC. *Genome Res*. 2002;12:996-1006.

29. Vogelstein B, Papadopoulos N, Velculescu VE, Zhou S, Diaz LA, Kinzler KW. Cancer genome landscapes. *Science*. 2013;339:1546-1558.

30. Sanchez-Vega F, Mina M, Armenia J, et al. Cancer Genome Atlas Research Network. Oncogenic signaling pathways in The Cancer Genome Atlas. *Cell*. 2018;173:321-337.e10

31. Ding LI, Bailey MH, Porta-Pardo E, et al. Cancer Genome Atlas Research Network. Perspective on oncogenic processes at the end of the beginning of cancer genomics. *Cell*. 2018;173:305-320.

32. Forbes SA, Beare D, Boutselakis H, et al. COSMIC: somatic cancer genetics at high-resolution. *Nucleic Acids Res*. 2017;45:D777-D783.

33. Oda K, Okada J, Timmerman L, et al. PIK3CA cooperates with other phosphatidylinositol 3'-kinase pathway mutations to effect oncogenic transformation. *Cancer Res*. 2008;68:8127-8136.

34. Rudd ML, Price JC, Fogoros S, et al. A unique spectrum of somatic PIK3CA (p110alpha) mutations within primary endometrial carcinomas. *Clin Cancer Res*. 2017;17:1331-1340.

35. Simon MP, Pedeutour F, Sirvent N, et al. Deregulation of the platelet-derived growth factor B-chain gene via fusion with collagen gene COL1A1 in dermatofibrosarcoma protuberans and giant-cell fibroblastoma. *Nat Genet*. 1997;15:95-98.

36. Zhu K, Liu QI, Zhou Y, et al. Oncogenes and tumor suppressor genes: comparative genomics and network perspectives. *BMC Genom*. 2015;16(Suppl 7):S8.

37. Berger AH, Knudson AG, Pandolfi PP. A continuum model for tumour suppression. *Nature*. 2011;476:163-169.

38. Jain PK. Epigenetics: the role of methylation in the mechanism of action of tumor suppressor genes. *Ann N Y Acad Sci*. 2003;98:71-83.

39. Largaespada DA. Haploinsufficiency for tumor suppression: the hazards of being single and living a long time. *J Exp Med*. 2001;193:F15-18.

40. Richards S, Aziz N, Bale S, et al. Standards and guidelines for the interpretation of sequence variants: a joint consensus recommendation of the American College of Medical Genetics and Genomics and the Association for Molecular Pathology. *Genet Med*. 2015;17:405-424.

41. Andersson J, Sihto H, Meis-Kindblom JM, Joensuu H, Nupponen N, Kindblom L-G. NF1-associated gastrointestinal stromal tumors have unique clinical, phenotypic, and genotypic characteristics. *Am J Surg Pathol*. 2005;29:1170-1176.

42. Li J, Dang Y, Gao J, et al. PI3K/AKT/mTOR pathway is activated after imatinib secondary resistance in gastrointestinal stromal tumors (GISTs). *Med Oncol*. 2015;32:111.

43. Lagarde P, Perot G, Kauffmann A, et al. Mitotic checkpoints and chromosome instability are strong predictors of clinical outcome in gastrointestinal stromal tumors. *Clin Cancer Res*. 2012;18:826-838.

44. Croce CM. Oncogenes and cancer. *N Engl J Med*. 2008;358:502-511.

45. Bauer S, Duensing A, Demetri GD, Fletcher JA. KIT oncogenic signaling mechanisms in imatinib-resistant gastrointestinal stromal tumor: PI3-kinase/AKT is a crucial survival pathway. *Oncogene*. 2007;26:7560-7568.

46. Wang C-M, Huang K, Zhou YE, et al. Molecular mechanisms of secondary imatinib resistance in patients with gastrointestinal stromal tumors. *J Cancer Res Clin Oncol*. 2010;136:1065-1071.

47. Haller F, Gunawan B, von Heydebreck A, et al. Prognostic role of E2F1 and members of the CDKN2A network in gastrointestinal stromal tumors. *Clin Cancer Res*. 2005;11:6589-6597.

48. Merten L, Agaimy A, Moskalev EA, et al. Inactivating mutations of RB1 and TP53 correlate with sarcomatous histomorphology and metastasis/recurrence in gastrointestinal stromal tumors. *Am J Clin Pathol*. 2016;146:718-726.

49. Heinrich MC, Patterson J, Beadling C, et al. Genomic aberrations in cell cycle genes predict progression of KIT-mutant gastrointestinal stromal tumors (GISTs). *Clin Sarcoma Res*. 2019;9:3.

50. Henderson V, Smith B, Burton LJ, Randle D, Morris M, Odero-Marah VA. Snail promotes cell migration through PI3K/AKT-dependent Rac1 activation as well as PI3K/AKT-independent pathways during prostate cancer progression. *Cell Adh Migr*. 2015;9:255-264.

51. Chen M, Zhang H, Zhang G, et al. Targeting TPX2 suppresses proliferation and promotes apoptosis via repression of the PI3k/AKT/P21 signaling pathway and activation of p53 pathway in breast cancer. *Biochem Biophys Res Commun*. 2018;507:74-82.

52. Aiba Y, Yamazaki T, Okada T, et al. BANK negatively regulates Akt activation and subsequent B cell responses. *Immunity*. 2006;24:259-268.

53. Dam EM, Habib T, Chen J, et al. The BANK1 SLE-risk variants are associated with alterations in peripheral B cell signaling and development in humans. *Clin Immunol*. 2016;173:171-180.

54. Guo Q, Lu T, Chen Y, et al. Genetic variations in the PI3K-PTEN-AKT-mTOR pathway are associated with distant metastasis in nasopharyngeal carcinoma patients treated with intensity-modulated radiation therapy. *Sci Rep*. 2016;6:37576.

55. Janku F, Yap TA, Meric-Bernstam F. Targeting the PI3K pathway in cancer: are we making headway? *Nat Rev Clin Oncol*. 2018;15:273-291.

SUPPORTING INFORMATION

Additional supporting information may be found online in the Supporting Information section at the end of the article.